Transactions on Machine Intelligence 2(2) (2019) 59-75

ISSN Online: 2821-1693

Transactions on Machine Intelligence

Journal Homepage: https://tmachineintelligence.ir/index.php/TMI

Speckle Noise Reduction in Optical Coherence Tomography Images Using a Combination of Edge-Preserving Filters and Discrete Wavelet Transform

A. Fahmi Jafarqulukhani[1], M. Ghiyami[2,*], S. Jafari Namin[2]

[1] Department of Biomedical Engineering-Bioelectric, Faculty of Biomedical Engineering, Sahand University of Technology, Tabriz, Iran
[2] Assitant Professor, Department of Electrical Engineering, Ardabil Branch, Islamic Azad University, Ardabil, Iran
[3] Department of Electrical Engineering, Ardabil Branch, Islamic Azad University, Ardabil, Iran

ARTICLE INFO

Article History:
Received 10 April 2019
Received in revised form 3 May 2019
Accepted 8 June 2019
Available online 9 June 2019

Keywords:
Medical Image Processing, Discrete Wavelet Transform, Noise Reduction, Edge-Preserving Filter, Retinal Layers, Optical Coherence Tomography

ABSTRACT

Imaging techniques are repeatedly employed by radiologists to detect internal structural details and body function. Optical coherence tomography (OCT) is a significant non-invasive medical imaging modality used to examine the microstructure of biological tissues. In this study, images from 500 patients who visited Noor Clinic in Ardabil for OCT imaging of the retina were collected. Since OCT images suffer from speckle noise, edge-preserving filters were utilized for noise reduction. By subtracting the output of the filtered image from the original image, some of the original image information and noise remained in the output. To restore the remaining information, the output resulting from subtracting the original image from the filtered image was decomposed using the discrete wavelet transform and soft thresholding, and the remaining image information was added to the filtered image. Among the edge-preserving filters, the guided filter demonstrated the best performance with MSE, PSNR, and IQI values of 79.949, 28.41, and 0.984, respectively, whereas the proposed method achieved values of 19.825, 33.78, and 0.989, respectively. After extracting the image information and restoring it to the output of the edge-preserving filters, significant changes in quantitative noise reduction metrics were observed. Consequently, in this study, by employing guided, bilateral, and db8 wavelet filters, we achieved better performance in preserving the edges of OCT images compared to edge-preserving filters.

1. INTRODUCTION

Optical coherence tomography (OCT) was first introduced by Huang et al. in 1991. In OCT systems, light energy is used instead of sound signals, and image formation depends on the optical properties of tissue structures. Due to the high speed of light, direct measurement of the echo signal delay is not feasible; therefore, the OCT imaging system operates based on low-coherence interferometry [1]. OCT is a non-invasive, non-ionizing imaging

* Corresponding Author: mo.ghiamy@iau.ac.ir
Department of Electrical Engineering, Ardabil Branch, Islamic Azad University, Ardabil, Iran

http://dx.doi.org/10.47176/TMI.2019.59

technology capable of high-speed tomographic imaging of biological tissues at micrometer resolution [2, 3]. Medical imaging methods like OCT, which include a coherent light source, are considered one of the essential modalities in medical imaging due to their cost-effectiveness and safety. This type of imaging system plays a crucial role in clinical diagnosis, detecting tissue abnormalities, and demonstrating retinal diseases [4-6].

The most significant issue in OCT imaging systems is the presence of speckle noise in the acquired images. Speckle noise is an artifact that is present in most medical imaging systems, especially OCT, and limits the interpretation of the acquired images. The presence of speckle noise reduces image contrast and signal-to-noise ratio, thereby complicating the interpretation of morphological features necessary for clinical diagnosis [7]. As shown in Figure 1, images acquired from the retinal structure using OCT include layers such as the inner limiting membrane (ILM), nerve fiber layer (NFL), ganglion cell layer (GCL), inner plexiform layer (IPL), inner nuclear layer (INL), outer plexiform layer (OPL), outer nuclear layer (ONL), inner segments of photoreceptors (ISP), outer segments of photoreceptors (OSP), and retinal pigment epithelium (RPE). Interpretation of biometric properties of the eye is based on the segmentation and identification of important retinal layers. Therefore, edge and layer detection methods in retinal images must be performed with high accuracy. The presence of speckle noise in OCT images complicates the image processing required for the detection and segmentation of retinal layers [6, 8, 9]. A necessary task in the field of medical image processing is noise reduction, particularly speckle noise, in OCT images. Various physical methods have been employed for this purpose, most of which increase the imaging process time for the patient, thus emphasizing the importance of processing methods in speckle noise reduction in OCT images.

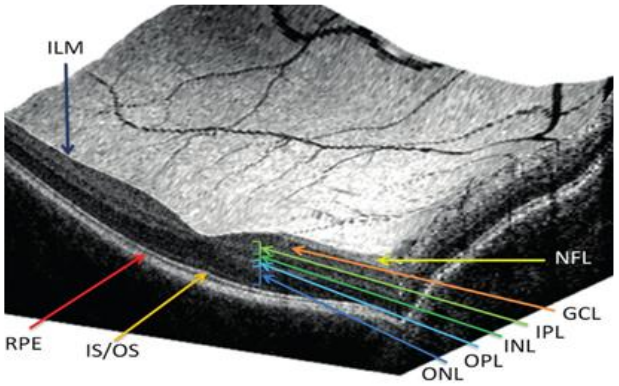

Fig.1. A 3D image of the retina acquired using an OCT imaging system, showing retinal layers [8].

Chi et al. [10] used fractional-order filtering and singular value shrinkage (SVS) to reduce speckle noise. In the proposed method, each OCT image is first divided into overlapping image blocks, and each block is filtered using a fractional mask. The absolute distance is used as a similarity criterion for block matching in the form of a low-rank matrix. Fractional-order processing is then applied to the obtained matrix, and singular value shrinkage is employed for reconstructing the filtered images. Wang et al. [11] introduced a two-stage iterative approach for speckle noise reduction. The proposed method employs the augmented Lagrange minimization for image recovery. The first stage of the iterative process removes added noise, while the second stage uses the SBM method to solve global variations in the noise removal problem. Bagheri et al. [12] introduced independent component analysis methods for speckle noise reduction in OCT images. Funk et al. [13] proposed a sparse representation-based image reconstruction method for OCT images and retinal layer segmentation. Fan et al. [14] presented an optimal OCT imaging method using a Hough transform-based noise reduction pattern. Esmaeili et al. [15] proposed a 2D curvelet transform-based dictionary learning method for speckle noise reduction in OCT images. Rashidi et al. [16] introduced an adaptive cluster-based filtering framework for speckle noise reduction in OCT skin images. Li et al. [17] employed a statistical model for speckle noise removal in OCT images. The proposed method suggests an optimal numerical framework based on MAP estimation. Rabbani et al. [18] employed an MMSE estimator for speckle noise reduction in 3D OCT data in the 3D wavelet domain. A prior distribution for the noise-reduced density function was introduced through the 3D wavelet, capable of modeling the main statistical properties of the wavelets.

In this paper, as shown in the block diagram in Figure 2, a method based on combining edge-preserving filters and discrete wavelet transform is proposed for speckle noise reduction in OCT images. The overall structure of this paper is as follows: In Section 2, edge-preserving filters, wavelet transform, and thresholding types are explained. Section 3 presents the implementation results, and Section 4 concludes with suggestions.

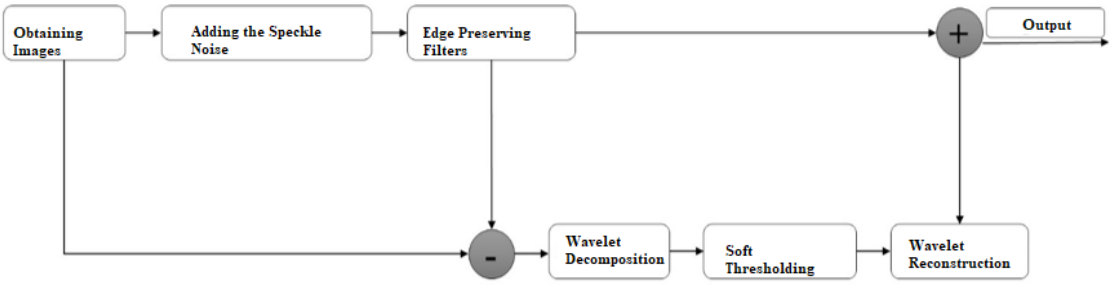

Fig.2. Block diagram of the proposed method for speckle noise reduction in optical coherence tomography images.

2. MATERIALS AND METHODS

2.1. Edge-Preserving Filters (EPF)

Edge-preserving filters are filters designed to reduce noise while retaining image edges and information. In other words, they smooth an image while preserving the edge details [19, 20]. There are various types of these filters, with the most important ones being the bilateral filter [21], the guided filter [22], and the anisotropic diffusion filter [23].

The bilateral filter is a nonlinear, non-iterative, and spatial method that defines gray levels or colors based on geometric proximity and photometric similarity. This filter preserves image edges by adjusting the weights of neighboring pixels. The bilateral filter is defined as follows:

$$\begin{cases} I_{BiLateral} = \dfrac{1}{W_P} \displaystyle\sum_{x_i \in \Omega} I(x_i) f_r(|I(x_i) - I(x)|) g_s(|x_i - x|) \\ W_p = \displaystyle\sum_{x_i \in \Omega} f_r(|I(x_i) - I(x)|) g_s(|x_i - x|) \end{cases} \quad (1)$$

Where $I_{BiLateral}$ ،Ω ،I ،x ،f_r and g_s represent the filtered image, a window centered at x , the current filter coordinates, the kernel function for smoothing intensity differences (which can be, for example, a Gaussian function), and the kernel function for smoothing coordinate distances (which can also be a Gaussian function), respectively. In the bilateral filter, fr and gs are modeled as Gaussian functions, and the filter's performance can be adjusted by setting the parameters σ_r and σ_s .

The guided filter is based on a spatial linear model where the computational cost is independent of the filter size. Theoretically, the guided filter assumes that the filter output O is the result of a linear transformation of the guidance image I in a spatial window W_k centered on pixel k:

$$O_i = a_k I_i + b_k \quad \forall i \in W_k \quad (2)$$

where Wk is a square window of size $(2r + 1) \times (2r + 1)$. The linear coefficients ak and bk are constant within Wk and can be estimated by minimizing the squared difference between the output image and the input image P:

$$\begin{cases} a_k = \dfrac{\frac{1}{|W|}\sum_{i\in W_k}(I_i P_i - \mu_k \overline{P_k})}{\delta_k + \epsilon} \\ b_k = \overline{P_k} - a_k \mu_k \end{cases} \tag{3}$$

where μ_k ، δ_k ، $|W|$ و $\overline{P_k}$ represent the mean of I , the variance of I , the number of pixels, and the mean of P in Wk , respectively. Subsequently, the output image is computed using equation (2). According to equation (3), all spatial windows centered on k in window W_i containing pixel i will contribute to the output image. Thus, the output changes each time Wk is recalculated. To address this, the mean coefficients ak and bk in equation (2) are averaged.

The anisotropic diffusion filter employs intra-region filtering instead of inter-region filtering. The main idea of this method is to convolve the input image with a Gaussian filter:

$$I(x, y, t) = I_0(x, y) * G(x, y; t) \tag{4}$$

Equation (4) represents a heat equation with the condition $I(x,y,0) = I_0(x,y)$. The anisotropic diffusion equation is described by equation (5):

$$I_{i,j}^{t+1} = I_{i,j}^{t} + \lambda[C_N \cdot \nabla_N I + C_S \cdot \nabla_S I + C_E \cdot \nabla_E I + C_W \cdot \nabla_W I]_{i,j}^{t} \tag{5}$$

where the operators ∇ and Δ represent the gradient and Laplacian with respect to space, respectively. The numerical form of the anisotropic diffusion filter is described by equation (6):

$$I_{i,j}^{t+1} = I_{i,j}^{t} + \lambda[C_N \cdot \nabla_N I + C_S \cdot \nabla_S I + C_E \cdot \nabla_E I + C_W \cdot \nabla_W I]_{i,j}^{t} \tag{6}$$

where $0 < \lambda < 1/4$. The gradient operator represents the nearest neighborhood difference via the following relation:

$$\begin{cases} \nabla_N I_{i,j} = I_{i-1,j} - I_{i,j} \\ \nabla_S I_{i,j} = I_{i+1,j} - I_{i,j} \\ \nabla_E I_{i,j} = I_{i,j+1} - I_{i,j} \\ \nabla_W I_{i,j} = I_{i,j-1} - I_{i,j} \end{cases} \tag{7}$$

The final image for high-contrast edges is obtained through equation (8):

$$g(\nabla I) = exp\left(-\left(\frac{\|\nabla I\|}{K}\right)^2\right) \tag{8}$$

Inverse filtering methods are not very effective in dealing with noise. In the Wiener filter [24], the image and noise are considered random variables, and the goal is to estimate the original image by minimizing the mean square error between them:

$$e^2 = E\left\{\left(f - \hat{f}\right)^2\right\} \tag{9}$$

Assuming that noise and the image are uncorrelated, one of them has zero mean, and the intensity levels in the estimation are linear functions of the degraded image's intensity levels. In this case, the minimum error function in the frequency domain is given by:

$$\hat{F}(u, v) = \left[\frac{1}{H(u, v)} \frac{|H(u, v)|^2}{|H(u, v)|^2 + S_\eta(u, v)/S_f(u, v)}\right] G(u, v) \tag{10}$$

where $H(u,v)$ ،$S_\eta(u,v)$ and $S_f(u,v)$ represent the degradation function, noise power spectrum, and undegraded image power spectrum, respectively. Wiener proposed that multiplying a complex quantity by its conjugate equals the square of its magnitude, known as the Wiener filter.

2.2. Image Decomposition Using Discrete Wavelet Transform

The fundamental principle in wavelet decomposition involves using scaling and translation functions. By scaling and translating, it is possible to detect signal features at different scales and cover all study areas. Therefore, a signal is decomposed into basis functions created from scaling and translating a base function (mother wavelet) [25]. In recent years, various wavelet families such as Daubechies [26], biorthogonal [27], and symmetric [26] wavelets have been introduced. Some wavelets, like biorthogonal wavelets, exhibit symmetry. The Haar wavelet is suitable for edge detection and binary pulse reconstruction. The Daubechies wavelet family is used for different applications, such as texture feature analysis, due to its orthogonal nature and finite length.

Assuming there exists an integrable scaling function (father wavelet) and a translation function (mother wavelet) in the space V_j and $W_j$such that any member function can be modeled by $\varphi(2^j t)$and $\psi(2^j t)$ [28]:

$$\begin{cases}\varphi_{j,k}(t) = 2^{j/2}\varphi(2^j t - k) \ \ , k = \cdots, -1,0,+1,\cdots \\ \psi_{j,k}(t) = 2^{j/2}\psi(2^j t - k) \ \ , k = \cdots, -1,0,+1,\cdots\end{cases} \tag{11}$$

Considering the nested spaces shown in Figure 3, the father and mother wavelets can be defined based on the weighted sum of the shifted scaling function [28]:

$$\begin{cases}\varphi(t) = \sum_n h[n]\sqrt{2}\varphi(2t-n) \ \ , n \in Z \\ \psi(t) = \sum_n g[n]\sqrt{2}\,\varphi(2t-n)\ n \in Z\end{cases} \tag{12}$$

where $h[n]$ and $g[n]$ represent the scaling function coefficients (scaling filter) and translation function coefficients (translation filter), respectively [29].

Since an image is a two-dimensional signal, a two-dimensional scaling function $\varphi(x,y)$and three two-dimensional wavelets (x,y) ،$\psi^V(x,y)$ ،$\psi^D(x,y)$ are required. Each wavelet produces a one-dimensional scaling function with the corresponding wavelet [25].

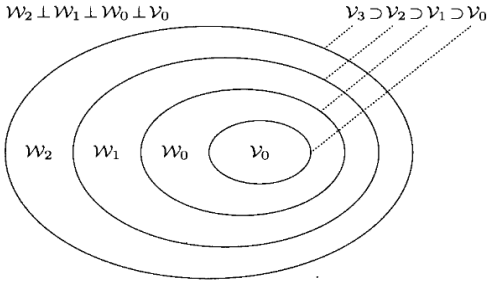

Fig.3. Illustration of the Scale Function and Wavelet Vector Space [29].

Since an image is a two-dimensional signal, a two-dimensional scaling function, $\varphi(x,y)$, and three two-dimensional wavelets, $\psi^H(x,y)$ ،$\psi^V(x,y)$ ،$\psi^D(x,y)$ are required. Each wavelet produces a one-dimensional scaling function with the corresponding wavelet [25]:

$$\begin{cases} \varphi(x,y) = \varphi(x)\varphi(y) \\ \psi^H(x,y) = \psi(x)\varphi(y) \\ \psi^V(x,y) = \varphi(x)\psi(y) \\ \psi^D(x,y) = \psi(x)\psi(y) \end{cases} \tag{13}$$

where ψ^H ،ψ^V و ψ^D measure horizontal variations along the image columns, vertical variations along the image rows, and diagonal variations, respectively. The two-dimensional scaling and translation basis functions are defined as follows:

$$\begin{cases} \varphi_{j,m,n}(x,y) = 2^{j/2}\varphi(2^j x - m, 2^j y - n) \\ \psi^i_{j,m,n}(x,y) = 2^{j/2}\psi^i(2^j x - m, 2^j y - n) \end{cases} \tag{14}$$

where i represents the mother wavelet in three directions: horizontal, vertical, and diagonal. For an image I(x,y) of size M×N, the discrete wavelet transform (DWT) is defined as follows [25]:

$$\begin{cases} W_\varphi(j_0,m,n) = \dfrac{1}{\sqrt{MN}} \displaystyle\sum_{x=0}^{M-1}\sum_{y=0}^{N-1} I(x,y)\varphi_{j_0,m,n}(x,y) \\ W_{\psi^i}(j,m,n) = \dfrac{1}{\sqrt{MN}} \displaystyle\sum_{x=0}^{M-1}\sum_{y=0}^{N-1} I(x,y)\psi^i_{j,m,n}(x,y) \end{cases} \tag{15}$$

Consequently, the inverse discrete wavelet transform (IDWT) is expressed as:

$$I(x,y) = \frac{1}{\sqrt{MN}}\sum_m\sum_n W_\varphi(j_0,m,n)\varphi_{j0,m,n}(x,y) + \frac{1}{\sqrt{MN}}\sum_i\sum_{j=j0}^{\infty}\sum_m\sum_n W_\psi(j_0,m,n)\,\psi^i_{j,m,n}(x,y) \tag{16}$$

The analysis and synthesis process in the discrete wavelet transform is illustrated in Figure 4. In this study, the filter bank decomposition was performed up to three levels.

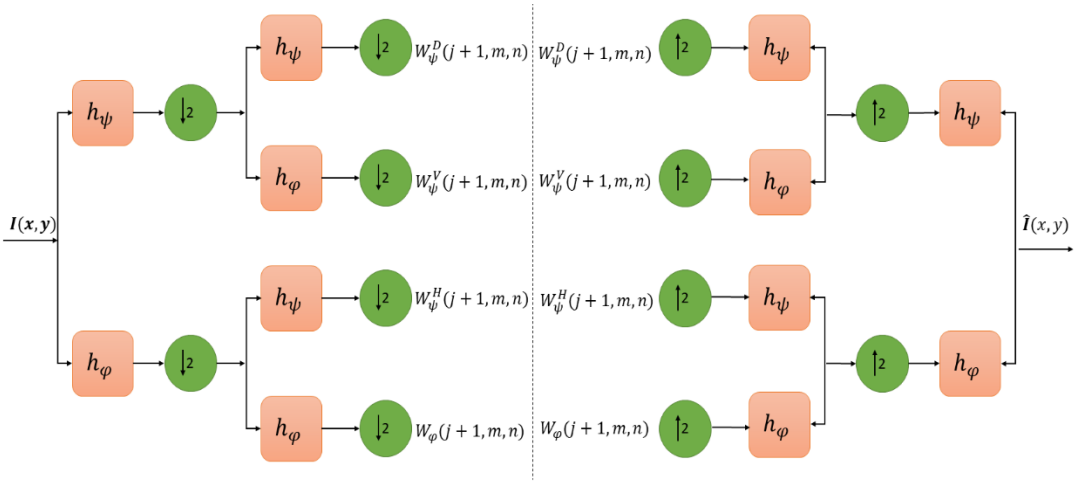

Fig.4. Illustration of the Analysis and Synthesis (Filter Bank Decomposition) in Discrete Wavelet Transform.

2.3. Wavelet Coefficient Thresholding

Wavelet thresholding is widely used for noise reduction in the wavelet domain. This method was introduced by Donoho and Johnston in 1994. In the wavelet domain, large coefficients usually represent signal information, while

small coefficients typically represent noise. By applying appropriate thresholding, the noise added to the signal can be reduced [30].

As shown in Figure 5, common wavelet thresholding is classified into two categories: hard thresholding and soft thresholding. The hard thresholding function is defined as follows [30]:

$$\begin{cases} Z = hard(\omega) = \omega, |\omega| > \lambda \\ Z = hard(\omega) = 0, |\omega| \leq \lambda \end{cases} \quad (17)$$

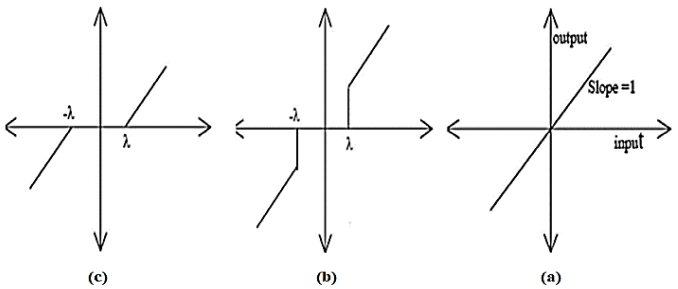

Fig.5. Types of Thresholding Functions. (a): Linear, (b): Hard, (c): Soft [30].

where ω and Z are the input and output wavelet coefficients, respectively. λ is a chosen threshold value. Similarly, the soft thresholding function is defined as follows [30]:

$$\begin{cases} Z = soft(\omega) = sgn(\omega)\, max(|\omega| - \lambda, 0)\,, |\omega| > \lambda \\ Z = soft(\omega) = 0, |\omega| \leq \lambda \end{cases} \quad (18)$$

Thresholding methods can be categorized into global thresholds and level-dependent thresholds. The first method applies a single threshold value λ to all wavelet coefficients, while the second method uses different thresholds for different levels. In this study, the soft thresholding method was employed.

3. IMPLEMENTATION RESULTS

To test the proposed method, images from Noor Ophthalmology Surgery Center in Ardabil were used. In this study, images from 500 patients who visited for OCT imaging of the macula and optic disc using the TOPCON OCT Triton device were utilized to evaluate the quantitative results of the proposed method. The imaging process and the OCT Triton device with the display system are shown in Figure 6. This device is capable of imaging the eye structure in both axial and three-dimensional cross-sectional views. It can measure posterior eye structures, including the retina, retinal nerve fiber layer, ganglion cell layer, inner plexiform layer, macula, optic nerve head, and choroid. The general features of the device are provided in Table 1. The scan speed of the device is 100,000 A-scans per second.

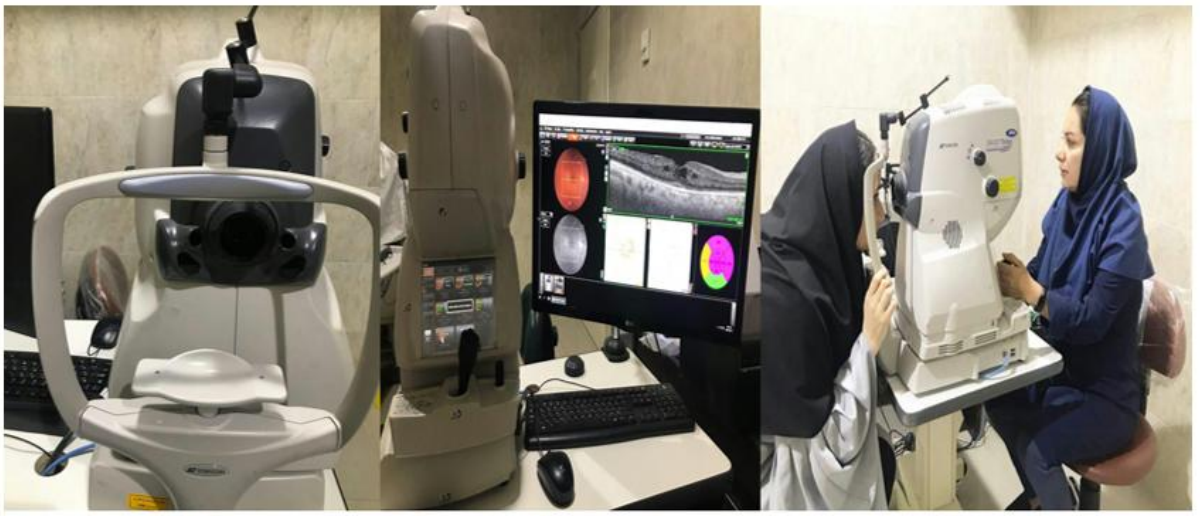

(c) (b) (a)

Fig.6. Illustration of the Imaging Process for the Macula Using the OCT Device at Noor Ophthalmology Surgery Center in Ardabil. (a): Setting Up the Device for Macula Imaging, (b): Device Adjustment System by Staff Along with the Display System, (c): Fixed Head Holder for Macula Imaging.

Table 1. General Characteristics of the OCT Device Used in the Noor Ardabil Eye Surgery Center

Features of laser light source				**Laser features**			
Corneal Output	Wavelength	Pulse Width	Beam Divergence	**Corneal Output**	Wavelength	Pulse Width	Beam Divergence
40 microwatts	1050 nanometers	6 microseconds	0.56 rad	1050 microwatts	1050 nanometers	6 microseconds	13 milliradians
Features LED output for front view				**Features of LED output for basic observations**			
Corneal Output	Wavelength	Beam Divergence	Pulse Width	Corneal Output	Wavelength	Beam Divergence	Pulse Width
200 microwatts	950 nanometers	0.06 radians	Continuous Wave	800 microwatts	850 nanometers	0.785 radians	Continuous Wave
LED light source features for front view				**LED light source features for basic observations**			
Output	Wavelength	Beam Divergence		Output	Wavelength	Beam Divergence	
14 milliwatts	950 nanometers	0.06 radians		135 microwatts	850 nanometers	0.52 radians	

To demonstrate the performance of the proposed method in reducing speckle noise from optical coherence tomography (OCT) images, three metrics are used: Peak Signal-to-Noise Ratio (PSNR), Mean Squared Error (MSE), and Image Quality Index (IQI). MSE is used as a measure of signal accuracy. The purpose of measuring signal accuracy is to compare two signals by providing a quantitative value to indicate the level of error or distribution between them. PSNR indicates the maximum signal power to the noise power present in the image. These two metrics are defined as follows [31]:

$$\begin{cases} MSE = \frac{1}{MN}\sum_{i=1}^{M}\sum_{j=1}^{N}\left[I(x,y) - \hat{I}(x,y)\right]^2 \\ PSNR = 10\,log_{10}\left(\frac{max(pixcell(I))^2}{MSE}\right) \end{cases} \tag{19}$$

The IQI metric is defined as the product of three terms: correlation loss, luminance distortion, and contrast distortion [32]:

$$IQI = \left(\frac{\sigma_{IB}}{\sigma_I \sigma_B}\right)\left(\frac{2m_I m_B}{{m_I}^2 + {m_B}^2}\right)\left(\frac{2\sigma_I \sigma_B}{{\sigma_I}^2 + {\sigma_B}^2}\right) \tag{20}$$

where [32]:

$$\begin{cases} m_I = \frac{1}{MN}\sum_{i=1}^{M}\sum_{j=1}^{N} I(i,j) \\ m_B = \frac{1}{MN}\sum_{i=1}^{M}\sum_{j=1}^{N} B(i,j) \\ {\sigma_I}^2 = \frac{1}{MN-1}\sum_{i=1}^{M}\sum_{j=1}^{N} (I(i,j) - m_I)^2 \\ {\sigma_B}^2 = \frac{1}{MN-1}\sum_{i=1}^{M}\sum_{j=1}^{N} (B(i,j) - m_B)^2 \\ \sigma_{IB} = \frac{1}{MN-1}\sum_{i=1}^{M}\sum_{j=1}^{N} (I(i,j) - m_I)(B(i,j) - m_B) \end{cases} \tag{21}$$

The final relationship for the IQI index is expressed as follows [32]:

$$IQI = \frac{4m_I m_B \sigma_{IB}}{({m_I}^2 + {m_B}^2)({\sigma_I}^2 + {\sigma_B}^2)} \tag{22}$$

where mI, mB, sigmaI, and sigmaB represent the mean of the original image, the mean of the filtered image, the variance of the original image, and the variance of the filtered image, respectively. The dynamic range for the IQI index is between [-1, +1], with the best result being IQI = 1. The measured quantities on the data set from the Noor Ardabil Eye Surgery Center are presented in Table 2. To further evaluate the proposed method, 80 OCT images from the data set [33] were used, and the measured quantities on these are shown in Table 3. In this paper, speckle noise with a variance of 0.05 was used to add noise to the OCT images. The idea in [32] inspired this paper, suggesting that applying a filter to reduce noise can result in the loss of some image information, while some noise information still remains. By employing edge-preserving filters, it is expected that the filtered image details, including textures or edges, will be noise-free, and the image information will not be lost during filtering.

However, as shown in Figure 7, subtracting the filtered image from the original image still leaves some noise and image information. Thus, to further reduce noise and restore the remaining image information, discrete wavelet transform was utilized. In this study, wavelets bior3.5, bior6.8, db8, db16, db20, sym8, sym16, coif5, and haar were used for this purpose. As seen in Table 2, among the images from the Noor Ardabil Clinic database, the guided and bilateral filters had the best performance when using edge-preserving filters. The proposed method showed that the best results for the PSNR and MSE criteria were achieved with the bilateral filter and db8 wavelet, while for the IQI criterion, the guided filter, bilateral filter, and bior3.5 wavelet performed best.

These results were also observed in the data set [33]. The best results for PSNR, MSE, and IQI in this data set were achieved with the bilateral filter and db8 wavelet. From Tables 2 and 3, it is concluded that the bilateral and guided filters performed well in reducing noise and preserving the edges of OCT images. Additionally, for restoring the remaining image information after applying these filters, the db8 wavelet showed the best performance. As shown in Figure 8, the speckle noise altered the histogram distribution of the noisy image compared to the original image. By applying edge-preserving filters (guided, anisotropic diffusion, and bilateral filters), as shown in the third-right column of Figure 8, we approximated the histogram distribution of the original image. However, by using the

discrete wavelet transform to decompose the image resulting from the subtraction of the filtered image from the original image and restoring the remaining information to the filtered image, a better estimation of the original image histogram distribution was achieved. In [32], Kumar used a non-local means filter (NLMF) instead of edge-preserving filters. This paper suggested using nonlinear filters instead of NLMF and applying the method to real images. The method proposed in [32] resulted in high MSE values, leading to a reduction in PSNR for OCT images from the Noor Ardabil Clinic. In medical image analysis, execution time and edge preservation are usually more important. One of the crucial parameters for edge preservation when applying filters to an image is the IQI parameter. Applying the method in [32] showed a low IQI parameter, and more importantly, the execution time for a single OCT image from the Noor Ardabil Clinic database averaged 150 seconds. Given the significance of edges in OCT images due to the embedded information of the retinal layers, edge-preserving filters were used to address the issues in the method proposed in [32].

Table 2. Average Values of PSNR, MSE, and IQI Using the Proposed Method for Reducing Speckle Noise from Optical Coherence Tomography (OCT) Images on 500 Sample Images from the Noor Ardabil Clinic Database

Method	PSNR	MSE	IQI	Method	PSNR	MSE	IQI
bior3.5	28.68	72.128	0.978	sym8	28.62	72.792	0.975
bior6.8	28.69	71.618	0.975	sym16	28.63	72.603	0.975
db8	28.56	73.826	0.974	coif5	28.64	72.583	0.975
db16	28.50	74.47	0.974	haar	28.10	82.829	0.972
db20	28.47	74.819	0.974				
Method	**PSNR**	**MSE**	**IQI**	**Method**	**PSNR**	**MSE**	**IQI**
MedianFilter	28.18	81.089	0.963	db8+MedianFilter	30.02	52.695	0.98
GuidedFilter	28.41	76.949	0.984	db8+GuidedFilter	31.31	42.366	0.986
WienerFilter	27.31	98.893	0.979	db8+WienerFilter	30.52	55.191	0.982
BilateralFilter	27.52	94.762	0.958	db8+BilateralFilter	33.78	19.825	0.989
DiffuseFilter	27.19	102.19	0.982	db8+DiffuseFilter	30.45	48.094	0.984
db16+MedianFilter	30.53	52.641	0.98	db20+MedianFilter	29.95	52.587	0.98
db16+GuidedFilter	31.26	42.155	0.986	db20+GuidedFilter	31.12	42.95	0.986
db16+WienerFilter	30.44	55.173	0.982	db20+WienerFilter	30.41	54.85	0.982
db16+BilateralFilter	31.72	41.534	0.987	db20+BilateralFilter	31.67	41.476	0.987
db16+DiffuseFilter	30.33	48.583	0.984	db20+DiffuseFilter	30.27	48.602	0.984
bior3.5+MedianFilter	32.43	33.825	0.986	bior6.8+MedianFilter	30.86	49.127	0.981
bior3.5+GuidedFilter	33.15	27.191	0.99	bior6.8+GuidedFilter	31.62	39	0.986
bior3.5+WienerFilter	32.51	34.02	0.987	bior6.8+WienerFilter	30.87	50.307	0.983
bior3.5+BilateralFilter	33.50	27.554	0.99	bior6.8+BilateralFilter	32.15	37.764	0.987
bior3.5+DiffuseFilter	32.56	28.991	0.989	bior6.8+DiffuseFilter	30.88	43.13	0.985
sym8+MedianFilter	30.64	51.901	0.98	sym16+MedianFilter	30.65	50.821	0.98
sym8+GuidedFilter	31.36	41.808	0.986	sym16+GuidedFilter	31.41	40.441	0.986
sym8+WienerFilter	30.58	54.408	0.982	sym16+WienerFilter	30.62	52.618	0.982
sym8+BilateralFilter	31.90	40.465	0.987	sym16+BilateralFilter	31.91	39.386	0.987
sym8+DiffuseFilter	30.57	46.76	0.984	sym16+DiffuseFilter	30.60	45.345	0.985
haar+MedianFilter	30.21	58.353	0.979	coif5+MedianFilter	30.66	51.042	0.98
haar +GuidedFilter	30.92	47.816	0.985	coif5+GuidedFilter	31.40	40.759	0.986
haar +WienerFilter	30.10	62.471	0.98	coif5+WienerFilter	30.61	53.049	0.982
haar +BilateralFilter	31.51	45.971	0.986	coif5+BilateralFilter	31.92	39.518	0.987
haar+DiffuseFilter	30.12	53.439	0.983	coif5+DiffuseFilter	30.60	45.52	0.984

Table 3. Average Values of PSNR, MSE, and IQI Using the Proposed Method for Reducing Speckle Noise from Optical Coherence Tomography (OCT) Images on 80 Sample Images from the Database [33]

Method	PSNR	MSE	IQI	Method	PSNR	MSE	IQI
bior3.5	28.85	75.04	0.972	sym8	28.19	84.658	0.967
bior6.8	28.35	82.534	0.968	sym16	28.22	85.927	0.966
db8	28.04	88.359	0.966	coif5	28.24	84.714	0.967
db16	27.84	91.179	0.965	haar	27.88	95.343	0.963
db20	27.83	93.587	0.964				
Method	**PSNR**	**MSE**	**IQI**	**Method**	**PSNR**	**MSE**	**IQI**
MedianFilter	27.55	102.293	0.930	db8+MedianFilter	29.32	67.862	0.972
GuidedFilter	29.14	71.869	0.981	db8+GuidedFilter	30.49	51.650	0.982
WienerFilter	28.24	87.824	0.976	db8+WienerFilter	29.76	65.161	0.977
BilateralFilter	28.41	85.122	0.947	db8+BilateralFilter	33.65	23.295	0.987
DiffuseFilter	28.15	90.658	0.98	db8+DiffuseFilter	29.81	60.609	0.980
db16+MedianFilter	29.07	68.764	0.972	db20+MedianFilter	29.19	69.322	0.972
db16+GuidedFilter	30.40	52.428	0.982	db20+GuidedFilter	30.37	54.214	0.982
db16+WienerFilter	29.67	66.225	0.977	db20+WienerFilter	29.64	66.643	0.977
db16+BilateralFilter	30.71	54.958	0.981	db20+BilateralFilter	30.66	55.427	0.982
db16+DiffuseFilter	29.67	62.254	0.980	db20+DiffuseFilter	29.62	62.831	0.980
bior3.5+MedianFilter	30.63	47.057	0.978	bior6.8+MedianFilter	29.42	64.354	0.973
bior3.5+GuidedFilter	31.85	37.125	0.985	bior6.8+GuidedFilter	30.67	49.150	0.982
bior3.5+WienerFilter	31.22	45.928	0.982	bior6.8+WienerFilter	29.97	61.878	0.977
bior3.5+BilateralFilter	32.18	38.861	0.985	bior6.8+BilateralFilter	31.05	50.811	0.981
bior3.5+DiffuseFilter	31.27	42.489	0.984	bior6.8+DiffuseFilter	30.07	56.781	0.981
sym8+MedianFilter	29.23	66.619	0.973	sym16+MedianFilter	29.24	66.597	0.972
sym8+GuidedFilter	30.53	50.998	0.982	sym16+GuidedFilter	30.54	50.834	0.982
sym8+WienerFilter	29.82	64.373	0.977	sym16+WienerFilter	29.82	64.184	0.977
sym8+BilateralFilter	30.90	52.898	0.981	sym16+BilateralFilter	30.89	52.788	0.981
sym8+DiffuseFilter	29.90	59.272	0.980	sym16+DiffuseFilter	29.89	59.313	0.980
haar+MedianFilter	29.10	69.112	0.972	coif5+MedianFilter	29.21	66.308	0.973
haar +GuidedFilter	30.44	52.447	0.982	coif5+GuidedFilter	30.54	50.677	0.982
haar +WienerFilter	29.71	66.517	0.977	coif5+WienerFilter	29.82	64.160	0.977
haar +BilateralFilter	30.80	54.642	0.981	coif5+BilateralFilter	30.90	52.599	0.981
haar+DiffuseFilter	29.87	60.488	0.980	coif5+DiffuseFilter	29.91	59.085	0.980

82	75	64	64	71	62	77	81	63	78	58
63	68	65	70	59	60	76	63	74	81	62
55	68	63	71	60	64	82	56	80	74	59
54	64	58	63	67	62	79	55	79	67	52
58	58	55	50	64	46	61	56	73	62	48
62	55	64	55	67	48	57	65	70	54	48
56	49	52	45	52	52	49	59	60	48	58
48	41	45	46	53	70	60	64	58	49	63
81	64	52	45	59	61	60	68	52	60	46
59	52	41	78	75	69	56	65	74	72	67

82	75	58	74	53	41	100	56	86	61	69
67	53	89	90	38	67	104	86	102	91	43
66	75	61	50	62	48	97	70	53	90	76
66	76	58	50	90	63	81	64	63	91	67
46	47	41	49	54	38	85	41	60	76	32
46	62	42	73	66	54	50	43	87	48	58
60	53	53	49	42	47	44	40	82	53	40
49	42	33	37	46	65	37	78	36	32	76
103	44	64	43	64	41	37	58	51	41	56
62	72	33	58	89	63	43	73	73	82	43

76	78	67	65	67	67	71	73	70	69	60
69	68	66	66	64	66	71	70	72	71	61
63	64	64	65	64	66	71	67	72	70	61
59	60	61	62	63	63	67	64	70	65	58
57	58	58	58	59	57	60	62	66	61	56
56	56	56	55	57	55	57	61	62	57	55
54	52	51	51	54	55	57	59	59	55	56
54	50	49	50	55	60	60	60	58	56	57
65	57	52	53	60	62	62	63	60	60	56
61	58	54	67	68	66	64	65	66	66	65

6	3	-3	-1	4	-5	6	8	-7	9	-2
-6	0	-1	4	-5	-6	5	-7	2	10	1
-8	4	-1	6	-4	-2	11	-11	8	4	-2
-5	4	-3	1	4	-1	12	-9	9	2	-6
1	0	-3	-8	5	-11	1	-8	7	1	-8
6	-1	8	0	10	-7	0	4	8	-3	-7
2	-3	1	-6	-2	-3	-8	0	1	-7	2
-6	-9	-4	-4	-2	10	0	4	0	-7	6
16	7	0	-8	-1	-1	-2	5	-8	0	-10
-2	-6	-13	11	7	3	-8	0	8	6	2

76	72	67	65	67	67	72	72	69	69	59
68	68	67	67	62	65	73	67	72	71	60
61	65	64	65	62	66	76	61	74	70	61
58	61	60	62	62	62	71	59	72	65	59
58	59	57	58	62	54	61	62	66	61	56
57	56	55	55	60	52	56	63	61	57	55
53	51	51	52	54	55	57	59	59	55	56
53	50	50	50	53	61	60	59	59	56	57
68	59	52	52	60	62	62	63	60	60	56
59	56	54	68	69	65	64	65	66	67	65

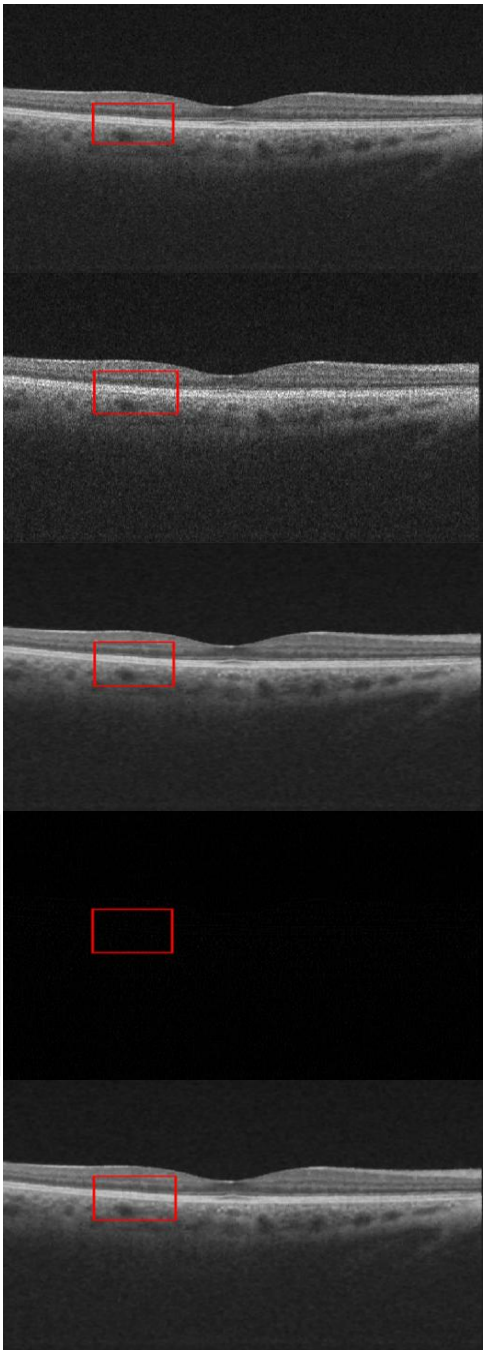

Fig. 7. Steps of the Proposed Method on a Sample from the OCT Database of Noor Ardabil Clinic. (First row): Original image, (Second row): Addition of speckle noise to the original image with a variance of 0.05, (Third row): Filtered image using a bilateral filter, (Fourth row): Difference between the original image and the filtered image, (Fifth row): Stage of restoring the remaining information to the filtered image.

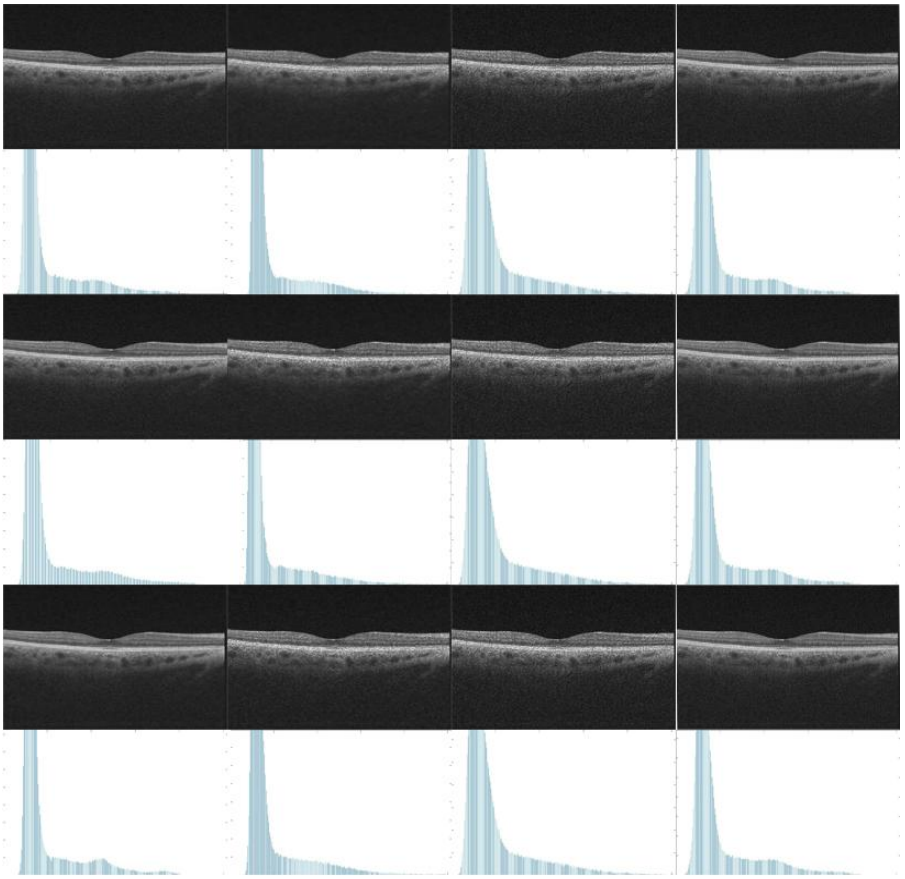

Fig. 8. A View of the Analysis of the Proposed Method Using Histograms from a Sample of the OCT Database of the Ardabil Noor Clinic. (First Column - Right): The Original Image Along with Its Histogram. (Second Column - Right): The Speckle Noise Image with Variance of 0.05 Along with Its Histogram. (Third Column - Right): The Output Images of the Guided Filters, Anisotropic Diffusion, and Bilateral Filters Along with Their Histograms. (Fourth Column - Right): The Output Images of the Proposed Method, GuidedFilter+Bior3.5, DiffusionFiltE

Table 4. Comparison of the Proposed Method (Combination of Bilateral Filter and db8 Wavelet) in Removing Speckle Noise with 0.05 Variance from Given Images with Method [32] (Combination of NLFM Filter with Various Wavelets)

Input image: Lena 512×512				Input image: Barbara 402×566		
Method	PSNR	IQI	Time (sec)	PSNR	IQI	Time (sec)
NLFM+db8	22.78	0.985	221.92	22.82	0.974	190.06
NLFM+db16	23.05	0.995	213.27	22.69	0.977	185.32
NLFM+sym8	22.94	0.987	211.39	22.84	0.976	200.61
NLFM+coif5	22.90	0.988	211.85	22.64	0.977	186.68
NLFM+bior6.8	22.32	0.967	214.02	22.04	0.970	182.77
Proposed: Bilateral+db8	**38.70**	**0.998**	**0.389**	**35.95**	**0.996**	**0.25**
Input image: Boat 512×512				Input image: Baboon 512×512		
Method	PSNR	IQI	Time (sec)	PSNR	IQI	Time (sec)
NLFM+db8	25.24	0.980	224.152	23.22	0.940	223.24
NLFM+db16	25.23	0.980	234.93	23.24	0.939	221.82
NLFM+sym8	25.35	0.980	212.35	23.30	0.939	211.81
NLFM+coif5	25.23	0.979	214.49	23.33	0.940	215.35

NLFM+bior6.8	24.11	0.970	212.22	22.59	0.934	214.85
Proposed: Bilateral+db8	**35.36**	**0.996**	**0.32**	**30.68**	**0.989**	**0.354**
Input image: Ardabil Noor Clinic (OCT 400×400)				Input image: OCT 400×400 [33]		
Method	PSNR	IQI	Time (sec)	PSNR	IQI	Time (sec)
NLFM+db8	25.72	0.977	154.61	28.02	0.932	344.36
NLFM+db16	25.74	0.978	158.71	28.05	0.934	330.07
NLFM+sym8	25.75	0.977	156.12	28.04	0.933	310.49
NLFM+coif5	25.73	0.977	161.76	28.02	0.931	303.36
NLFM+bior6.8	25.69	0.977	156.45	27.78	0.925	306.52
Proposed: Bilateral+db8	**32.81**	**0.990**	**0.21**	**34.21**	**0.964**	**0.47**

In the method presented by Mr. Kumar, applied to four images including Lena, Barbara, Boat, and Baboon, as seen in Table 4, the NLFM filter combined with wavelets such as db8, db16, sym8, coif5, and bior6.8 did not perform as well as the proposed method. In the proposed method, the program execution time is significantly lower compared to the method presented in [32]. For the Lena image with dimensions 512×512, using the NLFM filter with various wavelets took over 3 minutes, whereas in the proposed method, the time parameter was reduced to 0.32 seconds. Additionally, the average PSNR value for the four images used in [32] is around 24, while in the proposed method it is 34. The combination of the NLFM filter with various wavelets on a sample OCT image from the Noor Ardabil Clinic database yielded average PSNR values of 25, IQT of 0.97, and an elapsed time of 157 seconds. In the proposed method, using the Bilateral Filter and db8 wavelet, we were able to improve these parameters. The implementations in this paper were carried out on an AMD A10-7400p system with 4GB RAM at 3.4GHz and MATLAB 2019 software.

4. CONCLUSION AND RECOMMENDATIONS

Improving the quality of medical images has gained significant importance in medical image processing. The details of medical images, including textures and edges, play a crucial role in diagnosing types of lesions. One of the most important imaging modalities where image edges play a significant role in diagnosing diseases and abnormalities related to the retina is Optical Coherence Tomography (OCT) images. Segmentation and identification of retinal layers become challenging if the OCT images are noisy. Therefore, the primary goal of this paper is to reduce speckle noise, which is always present in OCT images. Given the importance of edge preservation in OCT image processing, edge-preserving filters such as Guided Filter, Bilateral Filter, and Anisotropic Diffusion Filter were used. Considering that some image information and noise remain in the output of the difference between the original and filtered images, this paper utilizes the Discrete Wavelet Transform (DWT) to decompose the desired output. After extracting image information and restoring it to the output of the edge-preserving filters, significant changes were observed in quantitative metrics such as PSNR, MSE, and IQI. Consequently, in this paper, by using Guided Filter, Bilateral Filter, and db8 Wavelet, we achieved better performance in preserving the edges of OCT images compared to edge-preserving filters alone. To more accurately estimate noise in the output stage of the difference between the original image and the filtered image by edge-preserving filters, methods based on estimators such as MAP, EM, etc., are suggested for future work. Additionally, given the importance of edges in OCT images, instead of using wavelet transform, other transforms such as Curvelet Transform, Contourlet Transform, etc., can also be considered in future work.

Transparency Statement

The data supporting this study are available upon reasonable request to the corresponding author, subject to ethical and confidentiality considerations.

Acknowledgments

We would like to express our gratitude to all individuals who contributed to this project.

Declaration of Interest

The authors declare that they have no competing interests.

Funding

This research received no specific grant from any funding agency, commercial, or not-for-profit sectors.

REFERENCES

[1] Born, M., & Wolf, E. (2013). Principles of optics: Electromagnetic theory of propagation, interference and diffraction of light. Elsevier.

[2] Du, Y., Liu, G., Feng, G., & Chen, Z. (2014). Speckle reduction in optical coherence tomography images based on wave atoms. Journal of Biomedical Optics, 19(5). https://doi.org/10.1117/1.JBO.19.5.056009

[3] Adabi, S., Turani, Z., Fatemizadeh, E., Clayton, A., & Nasiriavanaki, M. (2017). Optical coherence tomography technology and quality improvement methods for optical coherence tomography images of skin: A short review. Biomedical Engineering and Computational Biology, 8. https://doi.org/10.1177/1179597217713475

[4] Nowshiravan Rahatabad, F., & Farzaneh Bahalgerdy, E. (2015). Speckle noise reduction for the enhancement of retinal layers in optical coherence tomography images. Iranian Journal of Medical Physics, 12(3), 178-188.

[5] Duan, J., Lu, W., Tench, C., Gottlob, I., Proudlock, F., Samani, N. N., & Bai, L. (2016). Denoising optical coherence tomography using second order total generalized variation decomposition. Biomedical Signal Processing and Control, 24, 120-127. https://doi.org/10.1016/j.bspc.2015.09.012

[6] Darlow, L. N., Akhoury, S. S., & Connan, J. (2014). A review of state-of-the-art speckle reduction techniques for optical coherence tomography fingertip scans. In Seventh International Conference on Machine Vision (Vol. 9445). https://doi.org/10.1117/12.2180537

[7] Ozcan, A., Bilenca, A., Desjardins, A. E., Bouma, B. E., & Tearney, G. J. (2007). Speckle reduction in optical coherence tomography images using digital filtering. JOSA A, 24(7), 1901-1910. https://doi.org/10.1364/JOSAA.24.001901

[8] Stankiewicz, A., Marciniak, T., Dąbrowski, A., Stopa, M., Rakowicz, P., & Marciniak, E. (2017). Denoising methods for improving automatic segmentation in OCT images of the human eye. Bulletin of the Polish Academy of Sciences Technical Sciences, 65(1), 71-78. https://doi.org/10.1515/bpasts-2017-0009

[9] Liu, X., Yang, Z., & Wang, J. (2016). A novel noise reduction method for optical coherence tomography images. In 9th International Congress on Image and Signal Processing, BioMedical Engineering and Informatics (CISP-BMEI) (pp. 167-171). IEEE. https://doi.org/10.1109/CISP-BMEI.2016.7852702

[10] Chen, H., Fu, S., Wang, H., Li, Y., & Wang, F. (2019). Speckle reduction based on fractional-order filtering and boosted singular value shrinkage for optical coherence tomography image. Biomedical Signal Processing and Control, 52, 281-292. https://doi.org/10.1016/j.bspc.2019.04.033

[11] Wang, X., Yu, X., Liu, X., Chen, S., Chen, S., Wang, N., & Liu, L. (2018). A two-step iteration mechanism for speckle reduction in optical coherence tomography. Biomedical Signal Processing and Control, 43, 86-95.

https://doi.org/10.1016/j.bspc.2018.02.011

[12] Baghaie, A., D'souza, R. M., & Yu, Z. (2016). Application of independent component analysis techniques in speckle noise reduction of retinal OCT images. Optik, 127(15), 5783-5791. https://doi.org/10.1016/j.ijleo.2016.03.078

[13] Fang, L., Li, S., Cunefare, D., & Farsiu, S. (2016). Segmentation-based sparse reconstruction of optical coherence tomography images. IEEE Transactions on Medical Imaging, 36(2), 407-421. https://doi.org/10.1109/TMI.2016.2611503

[14] Fan, Y., Ma, L., Chang, W., Jiang, W., Luo, S., Zhang, X., & Liao, H. (2018). Optimized optical coherence tomography imaging with hough transform-based fixed-pattern noise reduction. IEEE Access, 6, 32087-32096. https://doi.org/10.1109/ACCESS.2018.2846728

[15] Esmaeili, M., Dehnavi, A. M., Rabbani, H., & Hajizadeh, F. (2017). Speckle noise reduction in optical coherence tomography using two-dimensional curvelet-based dictionary learning. Journal of Medical Signals and Sensors, 7(2), 86. https://doi.org/10.4103/2228-7477.205592

[16] Rashedi, E., Adabi, S., Mehregan, D., Conforto, S., & Chen, X. W. (2017). An adaptive cluster-based filtering framework for speckle reduction of OCT skin images. arXiv preprint arXiv:1708.02285.

[17] Li, M., Idoughi, R., Choudhury, B., & Heidrich, W. (2017). Statistical model for OCT image denoising. Biomedical Optics Express, 8(9), 3903-3917. https://doi.org/10.1364/BOE.8.003903

[18] Rabbani, H., Sonka, M., & Abramoff, M. D. (2013). Optical coherence tomography noise reduction using anisotropic local bivariate Gaussian mixture prior in 3D complex wavelet domain. Journal of Biomedical Imaging, 22. https://doi.org/10.1155/2013/417491

[19] Goyal, A., Bijalwan, A., & Chowdhury, M. K. (2012). A comprehensive review of image smoothing techniques. International Journal of Advanced Research in Computer Engineering & Technology, 1(4), 315-319.

[20] Pal, C., Chakrabarti, A., & Ghosh, R. (2015). A brief survey of recent edge-preserving smoothing algorithms on digital images. arXiv preprint arXiv:1503.07297.

[21] Tomasi, C., & Manduchi, R. (1998). Bilateral filtering for gray and color images. 98.

[22] Li, S., Kang, X., & Hu, J. (2013). Image fusion with guided filtering. IEEE Transactions on Image Processing, 22(7), 2864-2875. https://doi.org/10.1109/TIP.2013.2244222

[23] Punhani, P., & Garg, N. K. (2015). Noise removal in MR images using non-linear filters. In 6th International Conference on Computing, Communication and Networking Technologies (ICCCNT) (pp. 1-6). IEEE. https://doi.org/10.1109/ICCCNT.2015.7395234

[24] Wu, Q. Q., Lee, J. P., Park, M. H., Park, C. K., & Kim, I. S. (2014). A study on development of optimal noise filter algorithm for laser vision system in GMA welding. Procedia Engineering, 97, 819-827. https://doi.org/10.1016/j.proeng.2014.12.356

[25] Leal, A. S., & Paiva, H. M. (2019). A new wavelet family for speckle noise reduction in medical ultrasound images. Measurement, 140, 572-581. https://doi.org/10.1016/j.measurement.2019.03.050

[26] Daubechies, I. (1992). Ten lectures on wavelets. Siam. https://doi.org/10.1137/1.9781611970104

[27] Mallat, S. (1999). A wavelet tour of signal processing. Elsevier. https://doi.org/10.1016/B978-012466606-

1/50008-8

[28] Soman, K. P. (2010). Insight into wavelets: From theory to practice. PHI Learning Pvt. Ltd.

[29] Burrus, C. S., Gopinath, R. A., Guo, H., Odegard, J. E., & Selesnick, I. W. (1998). Introduction to wavelets and wavelet transforms: A primer (1st ed.).

[30] Naimi, H., Adamou-Mitiche, A. B. H., & Mitiche, L. (2015). Medical image denoising using dual tree complex thresholding wavelet transform and Wiener filter. Journal of King Saud University-Computer and Information Sciences, 27(1), 40-45. https://doi.org/10.1016/j.jksuci.2014.03.015

[31] Ndajah, P., Kikuchi, H., Yukawa, M., Watanabe, H., & Muramatsu, S. (2011). An investigation on the quality of denoised images. International Journal of Circuit, Systems, and Signal Processing, 5(4), 423-434.

[32] Kumar, B. S. (2013). Image denoising based on non-local means filter and its method noise thresholding. Signal, Image and Video Processing, 7(6), 1211-1227. https://doi.org/10.1007/s11760-012-0389-y

[33] Gholami, P., Roy, P., Parthasarathy, M. K., & Lakshminarayanan, V. (2018). OCTID: Optical coherence tomography image database. arXiv preprint arXiv, 2018.